Semnan University

Mechanics of Advanced Composite Structures

Journal homepage: https://macs.semnan.ac.ir/

ISSN: 2423-7043

Research Article

Advanced FEA simulation of Mode II Interlaminar Fracture in Flax/Epoxy Multidirectional Laminate Composites Using the End-Notched Flexure (ENF) Test

Muhammad Syaiful Fadly [a*], Mirza Pramudia [b], Binsar Maruli Tua Pakpahan [c], Fajar Paundra [d]

[a] Department of Mechanical Engineering, Faculty of Engineering, Universitas Tadulako, Palu, Indonesia

[b] Department of Industrial and Mechanical Engineering, Faculty of Engineering, Universitas Trunojoyo Madura, Bangkalan, Indonesia

[c] Department of Mechanical Engineering Education, Faculty of Engineering, Universitas Negeri Medan, Medan, Indonesia

[d] Department of Mechanical Engineering, Faculty of Industrial Technology, Institut Teknologi Sumatera, Lampung, Indonesia

ARTICLE INFO

Article history:

Received: 2023-10-19

Revised: 2024-03-22

Accepted: 2024-05-12

Keywords:

Finite element analysis;

Mode II interlaminar fracture;

Flax/epoxy;

Multidirectional laminates;

End-notched flexure.

ABSTRACT

This study investigates the mode II interlaminar fracture mechanisms of flax/epoxy multidirectional laminates through finite element analysis (FEA) using the end-notched flexure (ENF) test. The laminates were configured as $[(0_2/\theta)_6/0_2]$ with θ = 0°, 45°, and 90°, designed to minimize elastic couplings, although off-axis orientations introduced localized effects of limited significance. Fiber orientations perpendicular to the crack plane generated distinct shear energy dissipation patterns, although mode II remained dominant. Quantitative analysis revealed that the 0° configuration exhibited a higher Mode II strain energy release rate (G_{II}) than the 45° and 90° configurations. In contrast, the 45° orientation significantly reduced the magnitude of G_{II} due to shear–extension coupling and mixed-mode interactions. The ±45° fiber orientation also induced a redistribution and instability of the interlaminar shear stress field, leading to localized concentrations of strain energy near the specimen edges. The FEA results consistently captured the sensitivity of the strain energy distribution to the stacking sequence and confirmed Mode II as the primary fracture propagation mechanism in flax/epoxy laminates under ENF loading.

1. Introduction

There has been a growing trend in the utilization of natural fiber-based composites across various engineering applications, including sports equipment, the automotive industry, and marine structures, primarily due to their economic, technical, and ecological benefits [1, 2]. Among the different types of natural fibers, flax fiber is one of the most widely adopted, offering mechanical properties comparable to those of glass fibers, which are commonly employed as reinforcement materials [3]. Consequently, the mechanical behavior of flax/epoxy composites has attracted considerable research attention over the past two decades [4-6].

Several studies have demonstrated that hybrid composites, which integrate natural and synthetic fibers within a polymer matrix, can enhance the overall performance of composite materials [7-9]. Dhakal et al. [10] investigated the effect of carbon fiber hybridization on the mechanical properties of flax laminates. They reported significant improvements in the tensile and flexural properties of carbon/flax hybrid composites compared to pure flax composites. In addition, several experimental studies have examined the mechanical behavior, damage mechanisms, impact resistance, and water

* **Corresponding author.**
E-mail address: msfadly@untad.ac.id

Cite this article as:
Mohammadi, A. and Mahdi-Nia, M., 2025. Title of article. *Mechanics of Advanced Composite Structures*, 12(1), pp. xx-xx
https://doi.org/10.22075/MACS.2024.39315.2050

absorption characteristics of carbon/flax/epoxy and glass/flax/epoxy hybrid composites [11-14]. Collectively, these findings indicate that the incorporation of glass or carbon fiber layers into flax/epoxy composites substantially enhances their mechanical performance.

In addition, various studies have explored the effects of interlayers, curing conditions, and temperature on the interlaminar fracture behavior of polymer composite laminates. Hosseini et al. [15] employed double cantilever beam (DCB) specimens to examine the effect of a mat layer at the delamination interface on the mode I fracture toughness of woven glass/epoxy laminates. The mat interlayer altered the crack propagation mechanism, reducing initiation and propagation fracture toughness by 80% and 69%, respectively, and fiber bridging was not the dominant toughening mechanism. Numerical simulations using a cohesive zone model validated by J-integral measurements accurately predicted the experimental load–displacement response.

Similarly, the effect of a thin mat layer between sub-laminates on mode II fracture toughness was studied using end-notched flexure (ENF) specimens [16]. Experimental results showed that the mat interlayer reduced the interlaminar fracture toughness for delamination initiation and propagation by 59% and 35%, respectively, while fiber bridging remained non-dominant in specimens without a mat interlayer. The influence of post-curing temperature on mode I fracture toughness was also examined. DCB specimens post-cured at 80°C and 100°C showed increases in initiation and propagation fracture toughness by 20–40% and 15–22%, respectively [17]. Increasing the test temperature further enhanced fracture toughness due to resin softening, improved ductility, and enlarged crack-tip plastic zones. Based on these findings, a temperature-dependent tri-linear cohesive zone model was developed and implemented in Abaqus via a UMAT subroutine to simulate mode I delamination growth, showing excellent agreement with experimental data (prediction error of approximately 4%) [18].

One of the primary failure modes in fiber-reinforced composites is delamination, which is considered one of the most critical and dangerous damage mechanisms in high-performance laminated composites. Consequently, extensive efforts have been devoted to characterizing delamination resistance, with the fracture mechanics approach emerging as the most widely adopted method [19, 20]. The double cantilever beam (DCB) test has been standardized for determining the mode I critical strain energy release rate (G_{Ic}) in unidirectional (UD) laminates with a stacking sequence of $[0°]_n$ [21-23].

Conversely, for mode II, several types of test specimens have been proposed; however, no consensus has yet been reached regarding the most reliable method [24]. Nevertheless, owing to its straightforward configuration, the ENF test has become the most widely adopted procedure for mode II characterization [25, 26]. Like mode I, the ongoing pre-standardization work generally employs UD specimens, which exhibit high stiffness and the ability to maintain stable crack growth, making them relatively ideal for interlaminar fracture testing. Nevertheless, most real-world applications involve multidirectional (MD) laminates, where delamination occurs between plies with different fiber orientations. Several studies have investigated mode II fracture behavior in MD laminates [27, 28].

The findings of these studies often reveal considerable discrepancies. For instance, the reported values of G_{IIc} for specimens with initial delamination at the θ/−θ interface have been observed to increase [29-31], decrease [32], or remain nearly unaffected by the ply angle θ [33]. These variations are primarily attributed to intra-ply damage and crack-jumping events that occur at neighboring interfaces. Conversely, for 0/θ specimens, G_{IIc} tends to decrease with increasing θ [22, 34], suggesting that UD specimens may not always provide the most conservative results.

The results reported in the literature often exhibit contradictions, particularly regarding the influence of fiber orientation and laminate configuration on the G_{IIc} values of multidirectional composites. Such inconsistencies represent one of the primary motivations for conducting the present numerical investigation. In this study, ENF tests were performed on MD flax/epoxy laminate specimens, with stacking sequences that had been previously analyzed using a three-dimensional FEA model. This approach is expected to provide a deeper understanding of mode II fracture behavior in MD natural fiber composites, while also addressing the knowledge gap concerning the relationship between laminate configuration, delamination mechanisms, and fracture resistance. Accordingly, the findings of this study are anticipated to serve as a reference for optimizing the design of natural fiber–based composites for engineering applications requiring high structural performance.

2. Materials and Methodology

2.1. Materials

Flax fibers were used as the reinforcement in the composite panels, with a density of 1.40 ± 0.18 g/cm^3. The matrix system consisted of an epoxy - hardener mixture, and the mechanical properties of the flax/epoxy laminates are summarized in Table 1.

Table 1. Material properties of flax/epoxy [35]

Type	Parameters	Value	Unit
Flax/ epoxy	Elastic modulus	E_{11} = 31.420 E_{22} = 5.580 E_{33} = 5.580 G_{12} = 2.021 G_{13} = 2.021 G_{23} = 2.070	GPa
	Poisson's ratio	ν_{12} = 0.353 ν_{13} = 0.38 ν_{23} = 0.353	

2.2. Methodology

The flax fibers were arranged in a multidirectional stacking sequence of $[(0_2/\theta)_6/0_2]$, with θ = 0°, 45°, and 90°. This configuration, consisting of 20 plies with a fiber volume fraction of 50%, was designed to minimize undesirable elastic couplings, as previously discussed [36]. The specimens were evaluated through FEA. Their dimensions are illustrated in Figure 1, with a width b = 20 mm, span 2L = 100 mm, crack length a = 25 mm, and total length of 160 mm, where the overall laminate thickness 2h = 6.5 mm, derived from the ply thickness of t = 0.15 mm. The numerical models were developed using the commercial finite element package ABAQUS®, as shown in Figure 2.

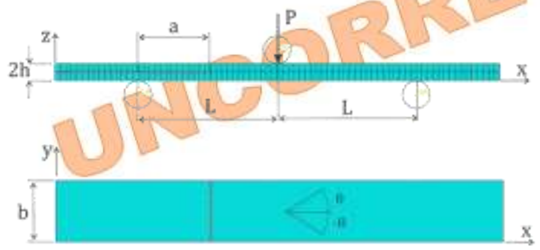

Fig. 1. Dimensions of ENF

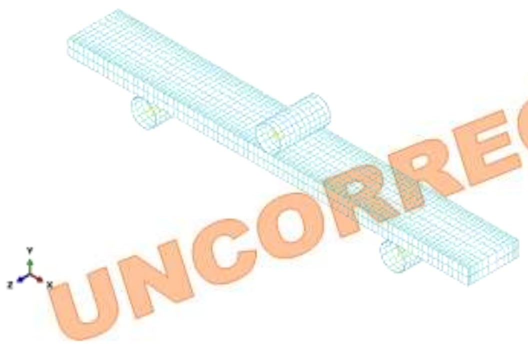

Fig. 2. Test setup for Mode II Delamination

To avoid interpenetration between the specimen arms, contact surfaces were carefully defined. In the present study, surface-to-surface contact was defined between the specimen and the cylindrical rollers. A friction coefficient of μ = 0.5 was adopted [36], and the resulting errors were found to be less than 2%. The strain energy release rate components (G_I, G_{II}, and G_{III}) were calculated using the Virtual Crack Closure Technique (VCCT) [37]. It has been well established that the stress field in the vicinity of delaminations between plies with different orientations exhibits an oscillatory nature [38]. The energy release rates for 2D and 3D cracks with low-order meshes are given in Equations 1–3:

$$G_I = -\frac{R_Y \Delta_v}{2\Delta A} \quad (1)$$

$$G_{II} = -\frac{R_X \Delta_u}{2\Delta A} \quad (2)$$

$$G_{III} = -\frac{R_Z \Delta_w}{2\Delta A} \quad (3)$$

Here, G_I, G_{II}, and G_{III} denote the mode I, II, and III energy release rates, respectively. The terms Δu, Δv, and Δw represent the relative displacements of the crack faces along the local x, y, and z directions, while R_X, R_Y, and R_Z are the corresponding nodal reaction forces. ΔA refers to the crack extension in 2D or the crack extension area in 3D (see Figure 3).

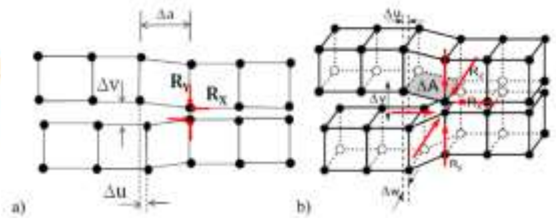

Fig. 3. Crack geometry schematics for: (a) 2D and (b) 3D models [39]

Crack growth modeling requires a fracture criterion for initiation and propagation. In linear elastic fracture mechanics (LEFM), this criterion is typically expressed in terms of critical energy release rates. In this study, a linear function of the fundamental modes was applied as follows:

$$f = \frac{G_I}{G_I^c} + \frac{G_{II}}{G_{II}^c} + \frac{G_{III}}{G_{III}^c} \quad (4)$$

Here G_I^c, G_{II}^c. G_{III}^c denotes the critical energy release rates for modes I, II, and III, respectively. It should be noted that the VCCT is limited by its need for a predefined crack front, which restricts its use in cases such as delamination propagation under impact. Previous studies on UD specimens [40] highlight the need to derive G_{IIc} from pre-cracks, as these values tend to be the most conservative. However, in mode II precrack tests, the exact crack length a is unknown, making compliance calibration necessary. FEA were utilized to verify the compliance calibration [41]:

$$C = C_0 + C_1 a + C_3 a^3 \quad (5)$$

$$G_{II} = \frac{P^2}{2b}(C_1 + 3C_3a^2) \quad (6)$$

where C_0, C_1, and C_3 are polynomial constants, P is the load, δ is the displacement, and a is fixed at 25 mm. A mesh convergence study was conducted using different element sizes to assess the stability of the predicted peak load and strain energy release rate. The graphical and quantitative results are presented in Figure 4 and Table 2, respectively.

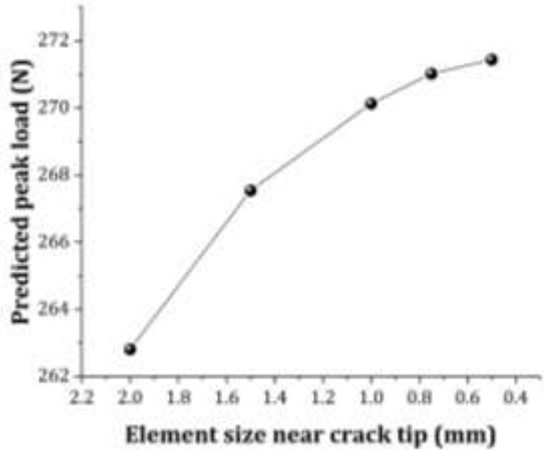

Fig. 4. Mesh convergence

Table 2. Summary of mesh convergence results

Mesh Level	Element Size Near Crack Tip (mm)	Number of Elements	Predicted Peak Load (N)	Change (%)	G_{II} (J/m^2)
M1	2.0	18425	262.81	–	18424
M2	1.5	26783	267.54	1.75	18931
M3	1.0	39659	270.13	0.96	19216
M4	0.75	52844	271.02	0.33	19361
M5	0.5	74327	271.44	0.15	19397

Figure 4 shows that when the element size is reduced to 0.5 mm, the variation in peak load becomes very small (<0.2%), indicating mesh independence at element sizes between 0.5 and 0.75 mm. Table 2 shows that the numerical response became increasingly stable with mesh refinement. In particular, when the element size near the crack tip was reduced from 0.75 mm to 0.5 mm, the variation in the predicted peak load was approximately 0.15%. In contrast, the variation in the G_{II} value was less than 0.2%. Therefore, a mesh with an element size of 0.75 mm near the crack tip was adopted as the convergence criterion to ensure mesh-independent, computationally efficient results. In addition, a mesh independence assessment was performed for the analysis step increment size, revealing negligible variations in the load-displacement response and G_{II} values with sufficiently small increments.

The ENF specimen was modeled as a three-dimensional deformable solid using eight-node, three-dimensional linear brick (C3D8) elements with a structured hexahedral mesh. Local mesh refinement was applied near the crack front to accurately capture the strain energy release rate using VCCT. The final element size near the crack tip was 0.75 mm. Mesh refinement was implemented using a biased seeding technique with a refinement ratio of 2:1 between the global mesh and the crack-front region. The ENF setup was simulated as a three-point bending configuration, where two cylindrical supports were defined as analytical rigid bodies and a vertical displacement load was applied through the central loading roller. Surface-to-surface contact was defined between the specimen and the rollers. The initial pre-crack (length a) was implemented by introducing a seam (debonded interface) along the laminate mid-plane over the specified crack length.

3. Results and Discussion

The load-displacement curves obtained during the fracture compliance test from the experimental results and FEA for the 0° orientation flax/epoxy composite are shown in Figure 5. It should be noted that the quantitative experimental validation in the present study was limited to the $[(0_2/0)_6/0_2]$ laminate configuration. However, the numerical predictions for the 45° and 90° configurations were performed using the same validated modeling framework, including identical material properties, boundary conditions, contact definitions, mesh refinement strategy, fracture criterion, and VCCT implementation. Therefore, the numerical trends observed for the off-axis configurations are considered physically consistent and suitable for a comparative analysis of the effect of fiber orientation on the distribution of the mode II strain energy release rate (G_{II}).

Figure 5(a) shows that both curves have the same trend, with an initial linear stage until reaching the peak load, followed by a decrease due to the initiation and propagation of mode II cracks. The maximum load value of the experimental results reached approximately 294.47 N, while the FEA results showed a peak load of approximately 271.10 N. This corresponds to a percentage difference of approximately 7.93%, indicating good agreement between the experimental and numerical results. Meanwhile, Figure 5(b) shows the stress distribution obtained from the FEA analysis of the ENF test specimen. The red color indicates the maximum stress concentrated in the initial crack area (notch), while the blue-to-green color gradation indicates lower stress levels in other parts. This distribution pattern is consistent with the mode II crack mechanism, where the dominant shear stress concentration occurs along the interlayer plane.

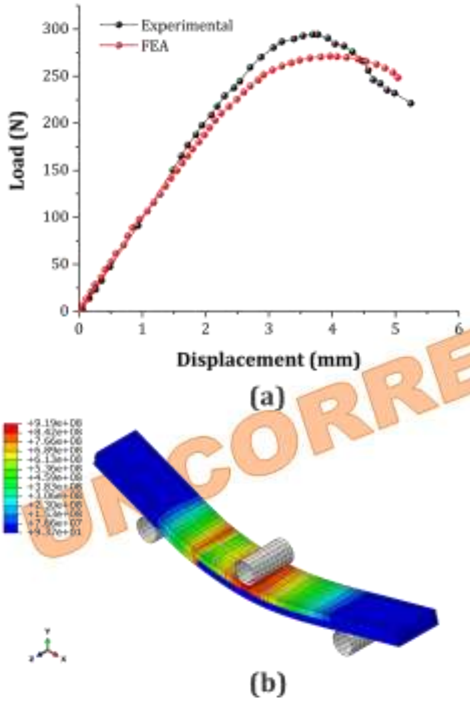

Fig. 5. (a) Load vs displacement curves and (b) FEA-based ENF tests

Figure 6(a) shows the distribution of mode I strain energy release rate (G_I) along the width of the ENF specimen. G_I values tend to be very low throughout the central area of the specimen, with significant increases occurring only at the edges. For example, in the $[(0_2/0)_6/0_2]$ configuration, the G_I value at the edges reaches 1.2 x 10^{-8} J/m^2, which is much higher than that in the central part, which is close to zero. Such a result is consistent with the theory that mode I contributions are very minimal in ENF testing due to the dominance of shear loading [26]. This relatively small G_I value confirms that the contribution of mode I fracture in the multidirectional flax/epoxy configuration is almost negligible compared to mode II. However, edge effects must still be taken into account.

In contrast, Figure 6(b) shows that mode II strain energy release rate (G_{II}) dominates the interlaminar response in the ENF test. For the $[(0_2/0)_6/0_2]$ laminate, the G_{II} value is relatively constant at around 19200 J/m^2, with a slight increase at the edge area to around 24000 J/m^2. Other configurations, such as $[(0_2/90)_6/0_2]$, show lower values, around 14500 J/m^2, indicating that fiber orientation significantly influences the interlaminar shear load-bearing capacity [42]. Meanwhile, in Figure 6(c), the mode III strain energy release rate (G_{III}) only provides a secondary contribution with a peak value of around 3762 J/m^2 at the edge and approaches zero at the center, indicating that mode III is only locally significant and not dominant. This distribution pattern is consistent with the classical theory of delamination, where G_{II} is the main controlling factor for crack propagation in the mode II ENF test [43]. At the same time, G_I and G_{III} play only minor roles.

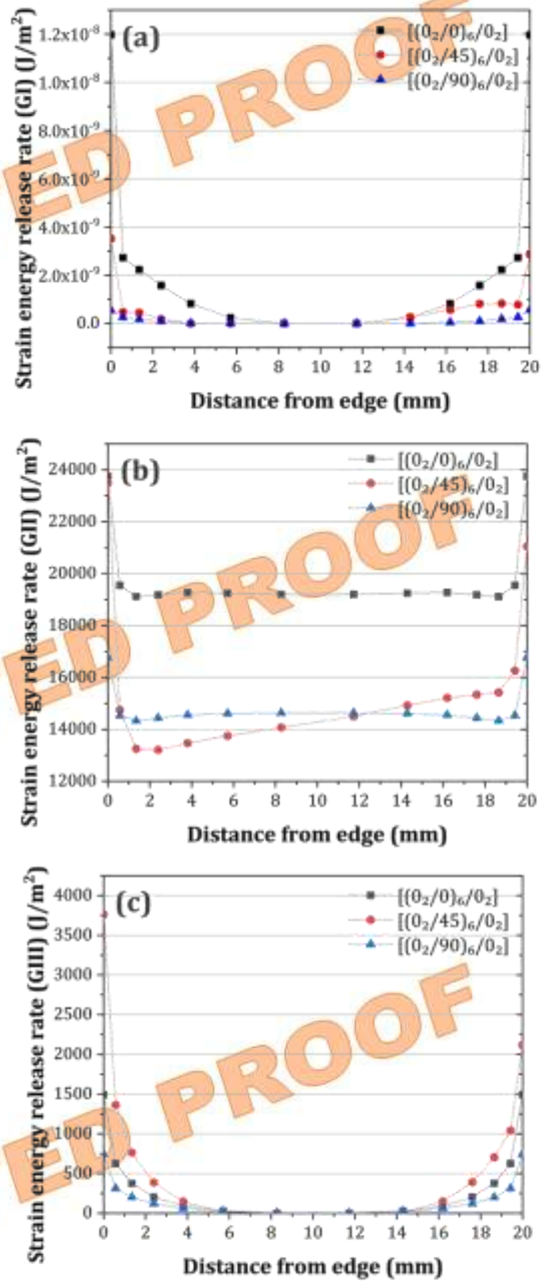

Fig. 6. Distribution of strain energy release rate along the width of ENF specimens: (a) G_I, (b) G_{II}, and (c) G_{III}

Figure 7 shows the GII distribution along the width of the specimens $[(0_2/0)_6/0_2]$, $[(0_2/45)_6/0_2]$, and $[(0_2/90)_6/0_2]$, which represent the limit case of elastic couplings [42]. The trend is relatively uniform in the center of the specimen, with significant deviations occurring only at the edges due to edge effects. The G_{II} values for the $[(0_2/0)_6/0_2]$ configuration tend to be stable in the range of 1.05–1.10 relative to the average value, indicating a nearly uniform distribution of strain energy release across the width. In contrast, the $[(0_2/45)_6/0_2]$ configuration exhibits greater variation, with a decrease to about 0.72 in the center and an increase to 1.30 at the edge regions. The result indicates that the presence of ±45° orientation causes instability in the interlayer shear stress distribution, which implies a higher concentration of strain energy release at the edge regions. Such a phenomenon can be explained through the fundamental equation for the strain energy release rate, where variations in effective width, as well as the contribution of fiber orientation to compliance, affect the consistency of the G_{II} distribution [44].

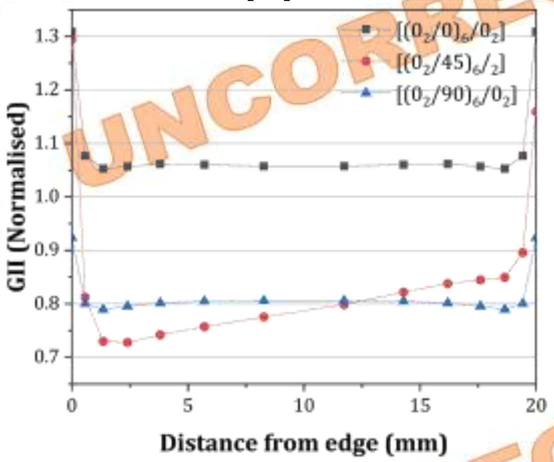

Fig. 7. G_{II} normalised with respect to the mean value along the width.

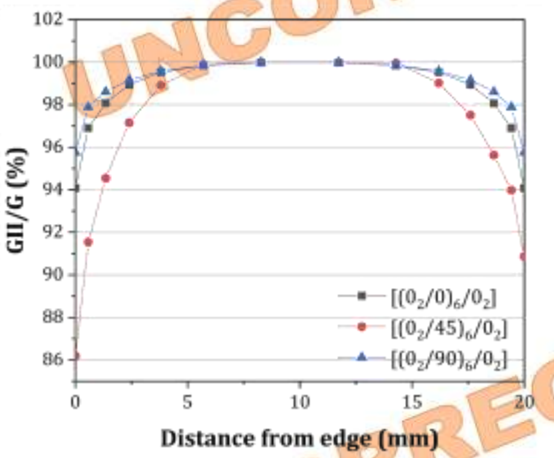

Fig. 8. Widthwise distribution of the mixed-mode ratio G_{II}/G in ENF specimens

Furthermore, the mode-mixity results in Figure 8 confirm the dominance of mode II, with the mode II component accounting for more than 96% of the total strain energy release rate, where $G = G_I + G_{II} + G_{III}$, on average. This finding confirms that the ENF configuration is well-suited to isolating pure mode II fracture in multidirectional flax/epoxy laminates, while also strengthening the reliability of advanced FEA simulations in capturing subtle variations across fiber orientations. Furthermore, the slight deviations in the $[(0_2/45)_6/0_2]$ configuration compared with those in the $[(0_2/0)_6/0_2]$ and $[(0_2/90)_6/0_2]$ configurations indicate that off-axis fiber orientations introduce local coupling effects, although these are not significant enough to alter the dominance of mode II energy release.

The special nature of the proposed specimens also requires validation of the test data reduction scheme. Various studies on UD specimens [43, 45] have demonstrated the importance of obtaining G_{IIc} values from pre-cracked specimens, as these are usually the most conservative. However, when testing mode II pre-cracked specimens, the exact crack length is not known beforehand, making a compliance calibration scheme crucial. One widely used scheme is ESIS compliance calibration [24].

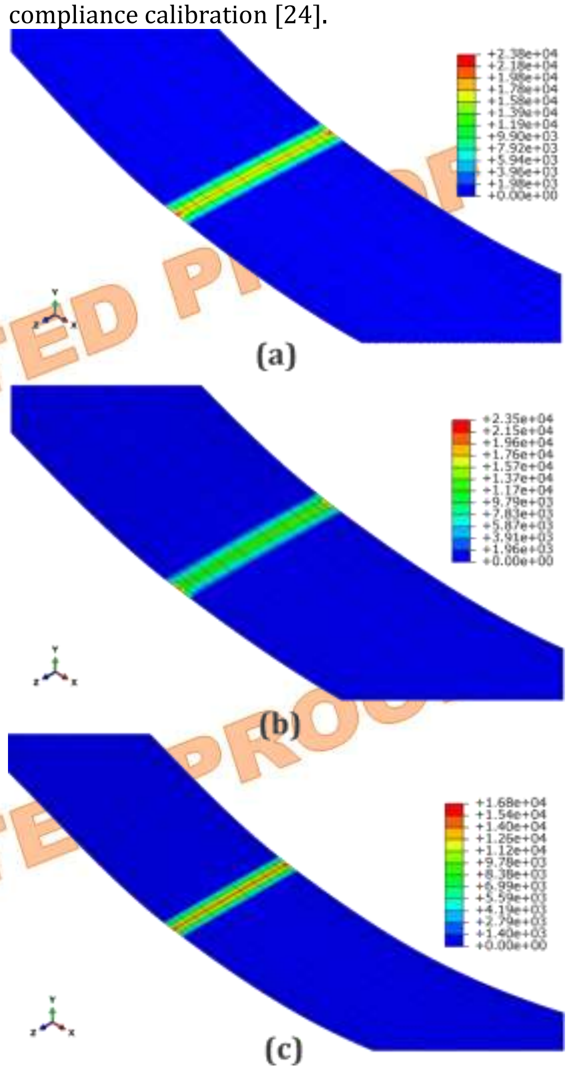

Fig. 9. Contour maps of the strain energy release rate (G_{II}): (a) $[(0_2/0)_6/0_2]$, (b) $[(0_2/45)_6/0_2]$, and (c) $[(0_2/90)_6/0_2]$

The G_{II} contour mapping results shown in Figure 9 illustrate the distribution of the interlaminar shear strain energy release rate for three multidirectional laminate configurations. In the $[(0_2/0)_6/0_2]$ specimen (Figure 9a), the G_{II}

concentration is relatively higher and uniformly distributed along the crack front, indicating efficient shear load transfer. This behavior occurs because the fiber orientation is parallel to the loading direction, allowing shear stresses to be effectively transmitted across the interface and concentrated at the crack tip.

In contrast, a significant reduction in G_{II} is observed in the $[(0_2/45)_6/0_2]$ configuration (Figure 9b). This reduction can be explained by the change in local stress state and deformation coupling induced by the off-axis ply orientation. Unlike the 0° laminate, where shear stresses are directly aligned with the fiber direction and efficiently transferred across the interface, the 45° orientation introduces strong shear–extension coupling effects. As shown in the contour maps, the 45° laminate exhibits a more diffused and redistributed. G_{II} field with lower intensity. This occurs because part of the applied shear loading is transformed into normal stress components due to the off-axis fiber orientation, reducing the effective shear driving force at the crack front and leading to mixed-mode interactions.

For the $[(0_2/90)_6/0_2]$ configuration (Figure 9c), the G_{II} distribution appears more localized with a moderate magnitude. The perpendicular fiber orientation relative to the crack plane alters the stiffness response and stress transfer mechanism. Although shear remains dominant, the energy dissipation mechanism differs from both the 0° and 45° cases due to the transverse stiffness characteristics of the laminate.

4. Conclusions

The FEA results of the ENF test demonstrate that mode II dominates the interlayer fracture behavior in multidirectional flax/epoxy laminates. The G_{II} distribution across the specimen width is generally uniform, with slight deviations at the edges. Importantly, variations in the stacking sequence significantly influence both the intensity and the distribution of shear energy. Among the configurations studied, $[(0_2/0)_6/0_2]$ exhibits the highest mode II strain energy release rate (G_{II}) and the most uniform distribution, indicating the strongest shear-driven crack propagation. In contrast, $[(0_2/45)_6/0_2]$ shows a notable reduction in G_{II} due to shear–extension coupling and mixed-mode interactions induced by the off-axis fiber orientation, while $[(0_2/90)_6/0_2]$ presents a more localized G_{II} distribution with a moderate magnitude. These results not only confirm that the ENF test combined with advanced numerical simulations can accurately capture the influence of fiber orientation on mode II fracture, but also provide new insights for optimizing natural fiber composite designs for high-performance structural applications.

Acknowledgments

The authors gratefully acknowledge the support provided by the Faculty of Engineering, Universitas Tadulako, in the completion of this research.

Conflicts of Interest

The authors declare that there is no conflict of interest regarding the publication of this article.

References

[1]. AL-Oqla, F. M., Hayajneh, M. T., and Nawafleh, N., 2023. Advanced synthetic and biobased composite materials in sustainable applications: a comprehensive review. *Emergent Materials*, 6(3), pp. 809–826.

[2]. Chauhan, V., Kärki, T., and Varis, J., 2022. Review of natural fiber-reinforced engineering plastic composites, their applications in the transportation sector and processing techniques. *Journal of Thermoplastic Composite Materials*, 35(8), pp. 1169–1209.

[3]. More, A. P., 2022. Flax fiber–based polymer composites: a review. *Advanced composites and hybrid materials*, 5(1), pp. 1–20.

[4]. Moudood, A., Rahman, A., Khanlou, H. M., Hall, W., Öchsner, A., and Francucci, G., 2019. Environmental effects on the durability and the mechanical performance of flax fiber/bio-epoxy composites. *Composites Part B: Engineering*, 171, pp. 284–293.

[5]. Ahmad, F., Yuvaraj, N., and Bajpai, P. K., 2021. Influence of reinforcement architecture on static and dynamic mechanical properties of flax/epoxy composites for structural applications. *Composite Structures*, 255, pp. 112955.

[6]. Saadati, Y., Lebrun, G., Chatelain, J.-F., and Beauchamp, Y., 2020. Experimental investigation of failure mechanisms and evaluation of physical/mechanical properties of unidirectional flax–epoxy composites. *Journal of Composite Materials*, 54(20), pp. 2781–2801.

[7]. Begum, S., Fawzia, S., and Hashmi, M. S. J., 2020. Polymer matrix composite with natural and synthetic fibres. *Advances in Materials and Processing Technologies*, 6(3), pp. 547–564.

[8]. Bakri, B., and Fadly, M. S., 2026. Investigation on Ballistic Impact

Properties of Rattan Fiber-Reinforced High-Density Polyethylene Composite Material. *International Journal of Engineering*, 37(1), pp. 1-9.
[9]. Fadly, M. S., Purnowidodo, A., Setyarini, P. H., Bakri, B., and Chandrabakty, S., 2024. Experimental and Numerical Modelling of Ballistic Impact on Fiber Metal Laminates Based on Aramid Fiber Reinforced Epoxy. *International Journal of Automotive and Mechanical Engineering*, 21(3), pp. 11554–11568.
[10]. Dhakal, H. N., Zhang, Z. Y., Guthrie, R., MacMullen, J., and Bennett, N., 2013. Development of flax/carbon fibre hybrid composites for enhanced properties. *Carbohydrate Polymers*, 96(1), pp. 1–8.
[11]. Manteghi, S., Sarwar, A., Fawaz, Z., Zdero, R., and Bougherara, H., 2019. Mechanical characterization of the static and fatigue compressive properties of a new glass/flax/epoxy composite material using digital image correlation, thermographic stress analysis, and conventional mechanical testing. *Materials Science and Engineering: C*, 99, pp. 940–950.
[12]. Bagheri, Z. S., El Sawi, I., Schemitsch, E. H., Zdero, R., and Bougherara, H., 2013. Biomechanical properties of an advanced new carbon/flax/epoxy composite material for bone plate applications. *Journal of the mechanical behavior of biomedical materials*, 20, pp. 398–406.
[13]. Al-Hajaj, Z., Sy, B. L., Bougherara, H., and Zdero, R., 2019. Impact properties of a new hybrid composite material made from woven carbon fibres plus flax fibres in an epoxy matrix. *Composite Structures*, 208, pp. 346–356.
[14]. Al-Hajaj, Z., Sarwar, A., Zdero, R., and Bougherara, H., 2019. In-situ damage assessment of a novel carbon/flax/epoxy hybrid composite under tensile and compressive loading. *Journal of Composite Materials*, 53(19), 2701–2714.
[15]. Hosseini, M. R., Taheri-Behrooz, F., and Salamat-talab, M., 2019. Mode I interlaminar fracture toughness of woven glass/epoxy composites with mat layers at delamination interface. *Polymer Testing*, 78, 105943.
[16]. Hosseini, M. R., Taheri-Behrooz, F., and Salamat-Talab, M., 2020. Mode II interlaminar fracture toughness of woven E-glass/epoxy composites in the presence of mat interleaves. *International Journal of Adhesion and Adhesives*, 98, 102523.
[17]. Esmaili, A., and Taheri-Behrooz, F., 2025. Post-curing effect on the mode I fracture toughness of the glass/epoxy laminates. *Polymer Composites*, 46(7), 6571–6581.
[18]. Esmaili, A., and Taheri-Behrooz, F., 2025. Temperature-dependent cohesive zone model for modeling mode I delamination of composite laminates under elevated temperature. *Theoretical and Applied Fracture Mechanics*, 140, 105176.
[19]. de Castro Saiki, L. E., and Gomes, G. F., 2024. Understanding and mitigating delamination in composite materials: a comprehensive review. *Mechanics of Advanced Materials and Structures*, 31(30), pp. 13147–13167.
[20]. Suriani, M. J., Rapi, H. Z., Ilyas, R. A., Petrů, M., and Sapuan, S. M., 2021. Delamination and manufacturing defects in natural fiber-reinforced hybrid composite: A review. *Polymers*, 13(8), pp. 1323.
[21]. Hawkins Jr, D. A., and Haque, A., 2015. Strain energy release rate and mode-I delamination growth in carbon-graphene/epoxy hybrid nanocomposites. *Procedia Engineering*, 105, pp. 829–834.
[22]. De Morais, A. B., De Moura, M. F., Gonçalves, J. P. M., and Camanho, P. P., 2003. Analysis of crack propagation in double cantilever beam tests of multidirectional laminates. *Mechanics of Materials*, 35(7), pp. 641–652.
[23]. Loh, L., and Marzi, S., 2018. An Out-of-plane Loaded Double Cantilever Beam (ODCB) test to measure the critical energy release rate in mode III of adhesive joints. *International Journal of Adhesion and Adhesives*, 83, pp. 24–30.
[24]. Blackman, B. R. K., Brunner, A. J., and Williams, J. G., 2006. Mode II fracture testing of composites: a new look at an old problem. *Engineering fracture mechanics*, 73(16), pp. 2443–2455.
[25]. Davies, P., Sims, G. D., Blackman, B. R. K., Brunner, A. J., Kageyama, K., Hojo, M., Tanaka, K., Murri, G., Rousseau, C., and Gieseke, B., 1999. Comparison of test configurations for determination of mode II interlaminar fracture toughness results from international collaborative test programme. *Plastics, rubber and composites*, 28(9), pp. 432–437.
[26]. Carlsson, L. A., Gillespie Jr, J. W., and Pipes, R. B., 1986. On the analysis and design of the end notched flexure (ENF) specimen for mode II testing. *Journal of composite materials*, 20(6), pp. 594–604.
[27]. Chai, H., 1990. Interlaminar shear fracture of laminated composites. *International Journal of Fracture*, 43(2), pp. 117–131.
[28]. Choi, N. S., Kinloch, A. J., and Williams, J. G., 1999. Delamination fracture of

multidirectional carbon-fiber/epoxy composites under mode I, mode II and mixed-mode I/II loading. *Journal of Composite Materials*, 33(1), pp. 73–100.

[29]. Yasaee, M., Mohamed, G., Pellegrino, A., Petrinic, N., and Hallett, S. R., 2017. Strain rate dependence of mode II delamination resistance in through thickness reinforced laminated composites. *International Journal of Impact Engineering*, 107, pp. 1–11.

[30]. Li, X., Hallett, S. R., and Wisnom, M. R., 2008. Predicting the effect of through-thickness compressive stress on delamination using interface elements. *Composites Part A: Applied Science and Manufacturing*, 39(2), pp. 218–230.

[31]. Zou, Z., Reid, S. R., Soden, P. D., and Li, S., 2001. Measurement of the critical energy release rate GIIC for filamentwound GRP pipes. *Composites Part A: Applied Science and Manufacturing*, 32(2), pp. 271–280.

[32]. Hwang, J. H., Kwon, O., Lee, C. S., and Hwang, W., 2000. Interlaminar fracture and low-velocity impact of carbon/epoxy composite materials. *Mechanics of composite materials*, 36(2), pp. 117–130.

[33]. Polaha, J. J., Davidson, B. D., Hudson, R. C., and Pieracci, A., 1996. Effects of mode ratio, ply orientation and precracking on the delamination toughness of a laminated composite. *Journal of Reinforced Plastics and Composites*, 15(2), pp. 141–173.

[34]. Tao, J., and Sun, C. T., 1998. Influence of ply orientation on delamination in composite laminates. *Journal of composite materials*, 32(21), pp. 1933–1947.

[35]. Ekeoseye, W. S., Kolasangiani, K., Oguamanam, D. C. D., and Bougherara, H., 2022. Mode II interlaminar fracture toughness of flax/glass/epoxy hybrid composite materials: an experimental and numerical study. *Journal of Natural Fibers*, 19(11), 4286–4300.

[36]. Pereira, A. B., and de Morais, A. B., 2004. Mode II interlaminar fracture of glass/epoxy multidirectional laminates. *Composites Part A: applied science and manufacturing*, 35(2), pp. 265–272.

[37]. Fawaz, S. A., 1998. Application of the virtual crack closure technique to calculate stress intensity factors for through cracks with an elliptical crack front. *Engineering Fracture Mechanics*, 59(3), pp. 327–342.

[38]. Chow, W. T., and Atluri, S. N. 1997. Stress intensity factors as the fracture parameters for delamination crack growth in composite laminates. *Composites Part B: Engineering*, 28(4), pp. 375–384.

[39]. Gliszczynski, A., and Wiącek, N., 2021. Experimental and numerical benchmark study of mode II interlaminar fracture toughness of unidirectional GFRP laminates under shear loading using the end-notched flexure (ENF) test. *Composite Structures*, 258, pp. 113190.

[40]. Davies, P., Ducept, F., Brunner, A. J., Blackman, B. R. K., and Morais, de A. B., 2021. Development of a standard mode II shear fracture test procedure. In ECCM-7: Seventh European Conference on Composite Materials. Realising Their Commercial Potential. (Vol. 2, pp. 9–15).

[41]. Davies, P., 1992. Protocols for interlaminar fracture testing of composites. European Structural Integrity Society: Polymer and Composites Task Group.

[42]. Leonel, E. D., Chateauneuf, A., and Venturini, W. S., 2012. Probabilistic crack growth analyses using a boundary element model: applications in linear elastic fracture and fatigue problems. *Engineering Analysis with Boundary Elements*, 36(6), pp. 944–959.

[43]. Al-Khudairi, O., Hadavinia, H., Waggott, A., Lewis, E., and Little, C., 2015. Characterising mode I/mode II fatigue delamination growth in unidirectional fibre reinforced polymer laminates. *Materials & Design*, 66, pp. 93–102.

[44]. Czarnocki, P., 2000. Effect of reinforcement arrangement on distribution of GI, GII and GIII along fronts of circular delaminations in orthotropic composite plates. *In European Structural Integrity Society* (Vol. 27, pp. 49–60). Elsevier.

[45]. Shivakumar, K. N., Panduranga, R., Skujins, J., and Miller, S., 2015. Assessment of mode-II fracture tests for unidirectional fiber reinforced composite laminates. *Journal of Reinforced Plastics and Composites*, 34(23), pp. 1905–1925.